The Astrophysical Journal, 670: L21–L24, 2007 November 20

THE NONSPHERICAL SHAPE OF BETELGEUSE IN THE MID-INFRARED

K. Tatebe, A. A. Chandler, E. H. Wishnow, D. D. S. Hale, and C. H. Townes
Space Sciences Laboratory and Department of Physics, University of California, Berkeley, CA 94720; tatebe@ssl.berkeley.edu, chandler@ssl.berkeley.edu, wishnow@ssl.berkeley.edu, david@isi.mtwilson.edu, cht@ssl.berkeley.edu
Received 2007 August 27; accepted 2007 October 3; published 2007 October 25

ABSTRACT

Three-telescope interferometric observations from the Infrared Spatial Interferometer (ISI) are reported at spatial frequencies that resolve the size and shape of the star Betelgeuse (α Ori) at a wavelength of 11.15 μm with a bandwidth of 0.18 cm^{-1}. The data include closure phase measurements, the first such measurements of a stellar disk in the mid-infrared. The data indicate a clear asymmetry of the stellar surface at these wavelengths. Mechanisms for generating the observed asymmetry via an elliptical shape or a hot spot near the southern limb of the star are discussed.

Subject headings: infrared: stars — stars: individual (alpha Orionis) — stars: late-type — techniques: interferometric

1. INTRODUCTION

Betelgeuse (α Orionis) is a semiregular M2Iab (supergiant) star and one of the largest and brightest stars in the sky as viewed from Earth, making it well suited for interferometric work. There is a long history of measurements studying its size and shape, beginning with Michelson & Pease (1921), who measured it to have a diameter of 47 mas at visible wavelengths. More recently, images resolving the stellar disk have been obtained in the ultraviolet using the *Hubble Space Telescope* (*HST*; Gilliland & Dupree 1996), using interferometry in the visible (Young et al. 2000) and with millimeter waves (Lim et al. 1998).

The measurements reported here were carried out at the Infrared Spatial Interferometer (ISI) on Mount Wilson. The telescopes of the ISI are contained in trailers that can be repositioned to a variety of configurations (Hale et al. 2003), and recently the telescopes were moved into a triangularly shaped array with 34, 36, and 40 m baselines. Interferences between signals from each pair of telescopes have a sine-wave response function on the sky with the spacing between maxima decreasing as the distance between the telescopes increases. For a given baseline, i.e., separation of two telescopes, the larger the stellar size the smaller the fringe contrast, termed "visibility," in the measured interference (Monnier 2003). The visibility is normalized to a maximum value of unity using calibrator stars of known size and shape, which were α Tauri and α Boötis. The present configuration of the ISI is able to measure visibilities along three different position angles simultaneously with spatial frequencies high enough to resolve the stellar disk. Thus, departures from circular symmetry can be gauged by comparing visibilities at the different orientations of each baseline. The phase of each fringe is also measured and is of particular importance since any point asymmetry (changes with respect to 180° rotation) of an object is reflected as a nonzero phase in the visibility. Atmospheric distortion prevents accurate measurement of individual phases, but the sum of all three phases, known as closure phase, is insensitive to these distortions (Baldwin et al. 1986). This makes closure phase useful in characterizing the asymmetry of an object.

2. MEASUREMENTS

This Letter reports observations on 2006 November 7–11, 15, 16, 20, and December 1, 7, and 20. The measured visibilities are stable over this time period, with variations less than the probable errors. Therefore, the star is assumed to change little over the reported observations, and all measurements are grouped together into one data set.

The data are shown in Figure 1. Visibility data from telescopes 1 and 2, baseline (1–2), are represented by red diamonds and baselines (2–3) and (3–1) by green triangles and blue squares, respectively. The average position angles of each baseline, measured in degrees east of north, are 263°, 23°, and 144° for baselines (1–2), (2–3), and (3–1), respectively. Closure phase measurements are the magenta circles plotted as a function of the spatial frequency of baseline (3–1). Each data point is an average of ~15 minutes of integration on the star.

The visibilities in Figure 1 are too low to be accounted for by the resolution of stellar structure alone. Previous ISI data at shorter baselines indicate that this is due to the presence of a dust shell surrounding the star (Bester et al. 1996). Later data, which are still unpublished, indicate that in 2003–2005 the dust contributes approximately 40% of the total intensity in the mid-infrared. This is consistent with the silicate features found in spectroscopic measurements (Harper et al. 2001). Dust shells are generally rather featureless at the high spatial frequencies reported here and should only have the effect of lowering all of the visibility measurements by the same amount. The visibilities in Figure 1 differ substantially between baselines, even at the same spatial frequencies. These variations clearly show the star to be more resolved in certain directions than others. That is, the star is larger in the directions having smaller visibilities, indicating departures from circular symmetry. Previous measurements have fit a circularly symmetric uniform disk (UD) with a diameter of 43 mas to the visibility curve of Betelgeuse in the *H* band (~1.65 μm) along position angles from 63° to 85° (Perrin et al. 2004) and a diameter of 53 mas in the *N* band (~10 μm) in an east-west direction (Weiner et al. 2003). A model of the current data should, ideally, be consistent with UD visibility curves along the position angles of the previous measurements and be reasonably consistent with the previously measured *N*-band diameter.

2.1. *Elliptical Model*

A uniform ellipse is a convenient model that is noncircularly symmetric but has a simple expression for its visibility curve. When regarded along a fixed position angle, it is identical in

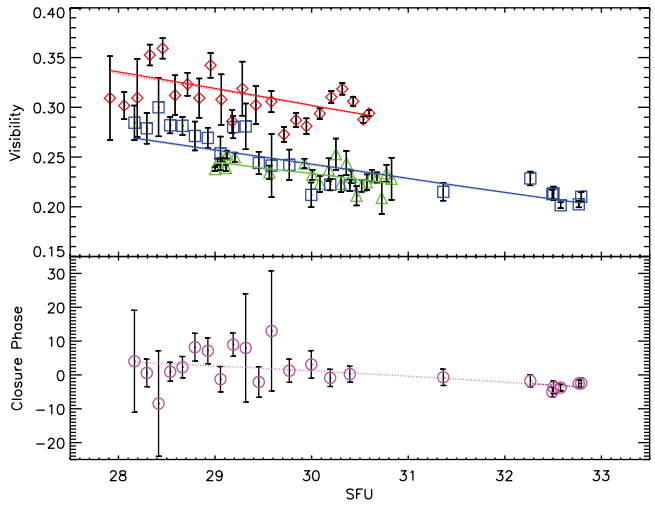

FIG. 1.—Visibility and closure phase data as a function of spatial frequency units (SFU $= 10^5$ cycles rad^{-1}). Modeled values are shown as solid and dotted lines for the images shown in Figs. 2 and 3, respectively. Data for baselines (1–2), (2–3), and (3–1) are colored red, green, and blue, respectively. The closure phases, in magenta, are plotted as a function of the spatial frequency of the (3–1) baseline.

shape to the visibility curve of a UD, but with a radius that varies depending along what position angle it is measured. The two-dimensional visibility function of an ellipse can be expressed analytically as

$$V(f, \theta) = C\left[\frac{J_1(2\pi f r(\theta))}{\pi f r(\theta)}\right], \quad (1)$$

where

$$r(\theta) = \sqrt{[(A^2 + B^2) + (A^2 - B^2)\cos(2\theta + \theta_0)]/2}. \quad (2)$$

In equation (1), $J_1(x)$ is a Bessel function of the first kind, f is the spatial frequency, θ is the position angle, and C is the calibration of the stellar component, i.e., the fraction of the visibility at zero spacial frequency due to the star only. In equation (2), θ_0 is the orientation of the major axis, and the lengths of the semimajor and semiminor axes are A and B, respectively. If $r(\theta)$ were a constant, then equation (1) would describe the visibility of a UD. The availability of an analytic expression allows least-squares fitting of the visibility data to be done much more efficiently than for visibility curves generated numerically.

A UD visibility curve is fitted to each of the visibility data points in Figure 1, giving fitted radii as a function of position angle. The function, $r(\theta)$, is then least-squares fitted to these radii. Errors are assigned to the radii based on the errors of the visibilities using standard error propagation methods. The fitted parameters are used to determine the dimensions and orientation of the ellipse. The resulting model is shown in Figure 2. The fitted UD radii, with errors, are plotted as a function of position angle around the ellipse. The UDs that would be fitted if the data of each baseline were regarded independently, i.e., if the star were assumed to be circular, are plotted as dotted circles, but only the elliptical model is consistent with data from all three baselines.

The parameters of the uniform ellipse model are given in Table 1 and agree reasonably well with the 26.33 mas radius

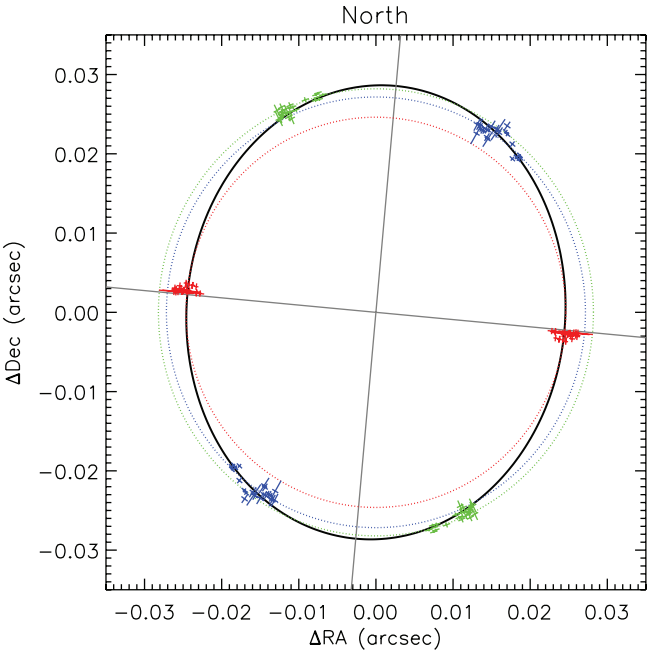

FIG. 2.—Ellipse fit to the visibility data of all three baselines, with the apparent size being shown by red, green, and blue crosses for the (1–2), (2–3), and (3–1) baselines, respectively. The modeled uniform disk radii for each measurement are plotted on both sides of the star, making each pair of clustered measurements redundant. Circular models fit to the measurements of each baseline individually are shown as dotted circles of corresponding color, so that deviations from circular models can be compared with probable errors in these measurements. The gray lines are aligned with the axes of the ellipse. North is up and east is left.

and 55.6% visibility fraction, which is the fraction from the star compared to the star and dust together, found previously by the ISI (Weiner et al. 2003). The current model of the star appears to be slightly larger and to contribute more of the total flux. The visibilities of the elliptical model, at the measured spatial frequencies and position angles, are found by Fourier transforming the elliptical image and are plotted as solid curves over the data shown in Figure 1. This model gives zero closure phases since it has point-symmetry; i.e., the ellipse is not lopsided and is roughly consistent with the measurements.

The elliptical shape might be most simply interpreted as an oblateness due to rotation, although this is inconsistent with

TABLE 1
MODEL PARAMETERS FOR α ORIONIS

Parameter	Ellipse	Circle and Point	Ellipse and Point
Reduced χ^2	2.91	2.60	2.50
Stellar fraction of flux (%)	61.8 ± 7.8	49.1 ± 1.6	54.4 ± 3.5
Semimajor axis (mas)	28.7 ± 0.05	24.2 ± 0.72	28.6 ± 5.6
Semiminor axis (mas)	24.5 ± 0.07	24.2 ± 0.72	26.8 ± 2.7
Orientation of major axis (deg)	−5.2 ± 1.5	...	7.3 ± 21.7
Fraction of flux from point (%)	...	5.3 ± 1.4	7.6 ± 3.7
Point location x (mas)	...	−2.19 ± 0.01	−2.4 ± 0.01
Point location y (mas)	...	−23.4 ± 0.01	−15.7 ± 0.01

NOTE.—Parameters for the models found in Figs. 2 and 3.

current estimates for the rotational speed of Betelgeuse (Uitenbroek et al. 1998). If the star is spinning fast enough, centrifugal forces will cause the star to bulge into an oblate spheroid. The surface of a spinning star is characterized by an equipotential contour with the potential determined by the gravitational and centrifugal contributions. Under the condition that the star deviates only slightly from spherical symmetry, the potential can be approximated as

$$U(R,\ \theta) = \frac{1}{2}\,\omega^2 R^2 \sin^2(\theta) + \frac{GM}{R}, \tag{3}$$

where ω is the angular velocity, G is the gravitational constant, and M is the mass of the star. Solving for the ratio of the polar to equatorial radius of such an equipotential surface yields, to first order

$$\frac{R_p}{R_e} \approx 1 - \frac{3\omega^2}{8G\pi\rho}. \tag{4}$$

A mass of 15 $M_\odot$ is assumed for Betelgeuse along with a radius of 5.59×10^{11} m (about 4.7 AU). The radius is based on the angular size from ISI measurements (Weiner et al. 2003) and a parallax from the *Hipparcos* satellite of 7.63 ± 1.64 mas (Perryman et al. 1997). This gives an average density, ρ, of 4.3×10^{-5} kg m^{-3}. The elliptical model shown in Figure 2 suggests that the equatorial radius (the semimajor axis of the ellipse) of Betelgeuse might be around 17% greater than the polar radius (the semiminor axis of the ellipse). For this case, and the above parameters, equation (4) can be solved for the rotation rate to give $\omega = 5.7 \times 10^{-8}$ rad s^{-1}, or a surface velocity of 31.8 km s^{-1}. This is about 5 times faster than current velocity estimates (Gray 2000; Uitenbroek et al. 1998), which indicate a period of 17 yr and would result in an oblateness of only 0.9%.

Since rotation cannot be assumed as the major source of asymmetry, other effects must be responsible. One possibility is that a pair of convection cells, each filling one hemisphere of the star, is responsible for a bipolar flow of material within it. Such a flow could account for the oblateness and has been found in finite element models of red giants (Jacobs et al. 1999). It is also possible that magnetic effects might contribute to the oblateness. The low surface gravity and potentially large magnetic activity from convection and rotation within the star suggests that this may be a plausible cause for significant variations in surface brightness (Dorch 2004). These variations in surface brightness, and possible distortions due to convection, could make the star appear elongated and elliptical without the need for rapid rotation.

2.2. *Hot Spot Model*

One alternative to effects that distort the shape of the star is a nonuniformity in the surface brightness. Hot spots have been observed on Betelgeuse in the visible (Young et al. 2000) but vanish at near-infrared wavelengths. This is probably because even modest increases in brightness at mid-infrared wavelengths require large changes in temperature. Thus, changes in the mid-infrared opacity of the outer layers of the star, thereby obscuring or revealing the much hotter lower layers, is a favored mechanism for such spots. The result from a model consisting of a uniform disk and a hot spot is shown in Figure 3. The point source provides a qualitative measure of the deviation from a symmetric circle and is used because an analytical expression for the visibility of such a model is available. This model also has the advantage over a pure ellipse of being able to generate nonzero closure phases, and Figure 1 shows the closure phase differs slightly from zero. The parameters for this model are also given in Table 1 along with the parameters for a model of an ellipse with a point source for comparison, although the latter is not plotted. The dotted circle in Figure 3 represents the size of a bright patch needed to match the modeled asymmetry if the patch has a surface brightness twice that of the star's surface. Clearly, the patch is too far offset to remain on the surface of the circular star. This may indicate that the patch is smaller or perhaps has a noncircular shape but is still near the edge of the star. Alternatively, the extra intensity generating the asymmetry may extend beyond the surface of the circular star, as might be the case for a large flare or other protuberance. The visibilities and closure phases of the circular model are plotted over the data as dotted lines in Figure 1. The visibilities of this model are generally similar to those of the pure ellipse. The fit to the closure phase, seen as a dashed magenta line in the bottom panel of Figure 1, shows that the model fits these data rather well. The reduced χ^2 for the fit to the visibility and closure phase data are comparable for both models; however, close examination of the closure phase data makes the importance of the asymmetry apparent. The average χ^2 per point for the fit to the closure phase data alone is only 0.91 for the asymmetric model but is 2.5 for any symmetric model with zero closure phases. This indicates that although both models oversimplify the images, as they are unable to fit small wiggles in the structure of the visibility data, the asymmetry produced by adding a point source is a statistically significant feature.

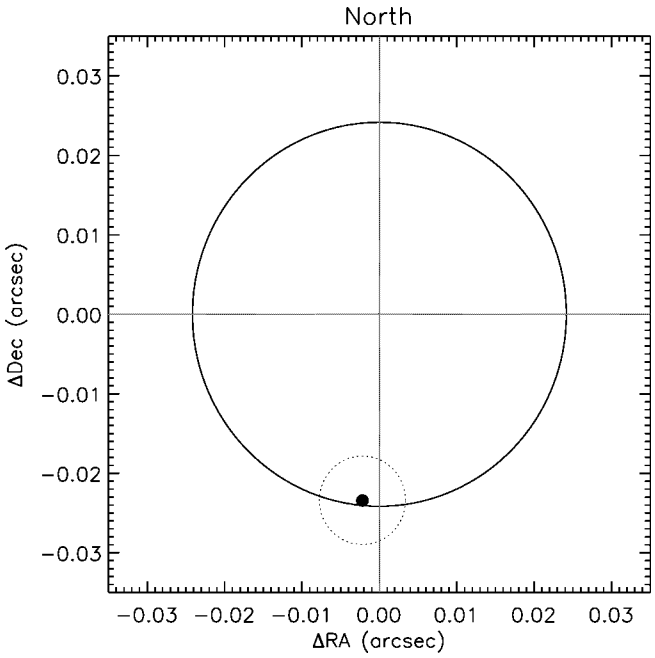

FIG. 3.—Circular model with a point source added to account for variation of visibility with position angle and closure phase measurements. The extra intensity in the point to the south-southeast is 5.3% of the total intensity. If the point has twice the flux of other parts of the star its size would be approximately the size shown by the dotted circle. North is up and east is left.

One complication in understanding the morphology of the star based on a hot spot model is that the stellar opacity source in the mid-infrared is not well understood. This makes it difficult to define what features of the star are being measured.

One possible source for mid-infrared opacity is free-free scattering of electrons off of neutral hydrogen atoms: H^-_{ff} scattering (Tatebe & Townes 2006). If this is the case, the opacity source in the mid-infrared and the millimeter wave should be the same, although the increased cross section at longer wavelengths would make millimeter-wave measurements sensitive to much lower densities of gas. This helps explain the size at 0.7 cm wavelength being roughly double that found in the mid-infrared (Lim et al. 1998). Warm water shells have also been suggested as a source of opacity (Ohnaka 2004; Tsuji 2006), but it is difficult for current models to generate lines broad enough to agree with no significant structure being seen in the spectra at ISI wavelengths (Weiner et al. 2003; Verhoelst et al. 2006). Furthermore, temperatures are high enough near the star that water may not be abundant. Both of these opacity sources are sensitive to temperature and can conceivably cause much greater fluctuations in the brightness than changes in blackbody emission alone. These opacities have opposite behaviors as a function of temperature. As temperature increases, the number of electrons ionized from metals increases, thereby increasing the opacity. This same increase in temperature would reduce the number of water molecules by dissociation, thereby reducing the opacity. Further studies of the star across multiple bands may help to resolve which is the dominant source of opacity. Finally, asymmetry due to the obscuring of the stellar disk by dust is also possible, although unlikely. Modeling of interferometric data in the near-IR shows very little limb darkening from dust for Betelgeuse (Perrin et al. 2004). Also, ISI closure phase measurements at shorter baselines indicate that the dust shell is quite symmetric, at least in the east-west direction, and are consistent with the east-west bilateral symmetry of the dust observed at 10 μm (Hinz et al. 1998). None of these measurements indicate features in the dust that could be expected to significantly alter the apparent geometry of the star.

3. CONCLUSION

To summarize, a pronounced asymmetry has been observed in the disk of Betelgeuse at mid-infrared wavelengths. This is in contrast to the rather uniform appearance of the star in the near-infrared around 1290 nm (Young et al. 2000). The pure ellipse model shown in Figure 2 is consistent with the elongation of an ellipse fit to measurements at a wavelength of 0.7 cm that show the star to be elongated in the northeast and southwest directions (Lim et al. 1998; Harper et al. 2001), although the apparent size is substantially larger at 0.7 cm wavelengths. It is unclear, however, what may cause this kind of elongation since centrifugal effects are not strong enough to produce the elongation modeled. The point source asymmetry shown in Figure 3 fits the data about as well as the elliptical model, although the closure phase data are fit significantly better. Also, the point source has approximately the same fractional brightness compared with the remainder of the star, and within about 10° of the position angle, as the bright feature found at 6500 Å by Goldberg et al. (1981). There is also a rough agreement with the orientation of the asymmetry in the *HST* image of Gilliland & Dupree (1996), which shows a spot to the southwest. These similarities indicate the asymmetry may be explained by a bright patch near the southern limb of the star possibly revealed by a reduced opacity in the outer layers of the star. The size of the patch is on the order expected of convection cells in red giants (Schwarzschild 1975), although the precise mechanism of opacity, and how it varies with turbulent or magnetic processes is unclear.

It is quite possible that the shape of the star is more complex than the models presented, as evidenced by the imperfect fits to details of the visibility curves. It is clear, however, that an excess of intensity to the south-southeast is required for consistency with ISI closure phase measurements. The exact shape and location of this asymmetry is, however, difficult to determine from these data. The small errors cited in Table 1 for the point source location suggest that the position is well constrained. These errors represent how rapidly χ^2 increases as the point is moved a small amount from its stated location. In reality, the behavior of χ^2 as the point source location varies is complex. While χ^2 increases rapidly in the immediate vicinity of the point, there are many nearby locations that give χ^2 values that are almost as small as the best fit. This can be clearly seen by the large change in point source location between the circular and elliptical star models despite the small errors listed for these locations. Generally, the best-fit point source locations were in the southern direction. Similarly, a change in the orientation of the pure ellipse model to $+7°$ shows only a modest increase in χ^2, although the fit for an orientation of 0° is very poor. Further study of this star in combination with theoretical and computer modeling, as well as a better understanding of opacity sources in the mid-IR, will help develop a more complete understanding of Betelgeuse and other red-giant stars.

We acknowledge use of *Hipparcos* data obtained from the Simbad database. We are very grateful for support from the Office of Naval Research, the National Science Foundation, and the Gordon and Betty Moore Foundation.

REFERENCES

Baldwin, J. E., Haniff, C. A., Mackay, C. D., & Warner, P. J. 1986, Nature, 320, 595
Bester, M., Danchi, W. C., Hale, D., Townes, C. H., Degiacomi, C. G., Mekarnia, D., & Geballe, T. R. 1996, ApJ, 463, 336
Dorch, S. B. F. 2004, A&A, 423, 1107
Gilliland, R. L., & Dupree, A. K. 1996, ApJ, 463, L29
Goldberg, L., Hege, E. K., Hubbard, E. N., Strittmatter, P. A. Cocke, W. J. 1981, SAO Special Report, 392, 131G
Gray, D. F. 2000, ApJ, 532, 487
Hale, D. D. S.et al. 2003, Proc. SPIE, 4838, 387
Harper, G. M., Brown, A., & Lim, J. 2001, ApJ, 551, 1073
Hinz, P. M., et al. 1998, Nature, 395, 251
Jacobs, M. L., Porter, D. H., & Woodward, P. R. 1999, BAAS, 31, 1447
Lim, J., Carilli, C. L., White, S. M., Beasley, A. J., & Marson, R. G. 1998, Nature, 392, 575
Michelson, A. A., & Pease, F. G. 1921, ApJ, 53, 249
Monnier, J. 2003, Rep. Prog. Phys., 66, 789
Ohnaka, K. 2004, A&A, 421, 1149
Perrin, G., Rideway, S. T., Coudé du Foresto, V., Mennesson, B., Traub, W. A., & Lacasse, M. G. 2004, A&A, 418, 675
Perryman, M. A. C., et al. 1997, A&A, 323, L49
Schwarzschild, M. 1975, ApJ, 195, 137
Tatebe, K., & Townes, C. H. 2006, ApJ, 644, 1145
Tsuji, T. 2006, ApJ, 645, 1448
Uitenbroek, H., Dupree, A. K., & Gilliland, R. L. 1998, AJ, 116, 2501
Verhoelst, T., et al. 1996, A&A, 447, 311
Weiner, J., Hale, D. D. S., & Townes, C. H. 2003, ApJ, 589, 976
Young, J. S., et al. 2000, MNRAS, 315, 635